20th Australasian Fluid Mechanics Conference
Perth, Australia
5-8 December 2016

Numerical Investigation of Wind Influence on the Focused Wave Group

D. Z. Ning, J. Du

State Key Laboratory of Coastal and Offshore Engineering Dalian University of Technology, Dalian 116024, China

Abstract

Wind and wave usually coexist in the real sea. Wind can greatly influence its kinematic and dynamic traits while the extreme wave occurs. In this study, a numerical model was developed to study the wind and extreme wave interaction based on potential flow theory. In the numerical model, the fully nonlinear kinematic and dynamic boundary conditions are satisfied on the instantaneous free surface. The extreme wave is generated at the certain spatial and temporal points using the wave focusing technique. Wind speed was introduced into the dynamic free surface boundary condition by making use of Jeffrey's sheltering mechanism. Besides, the mixed Eularian-Lagrangian technique was used to trace the transient free surface in the time-domain simulation. The boundary integral equation was founded based on the Second Green's Identity and resolved with the higher-order boundary element method. The numerical model was validated in comparison with the published experimental data. Then numerical tests were performed to study the wind influence on the characteristics of the focused wave group including derivations of focal time and position, focused wave height, the evolution process of wave focusing and defocusing, etc.

Introduction

With the further development in the offshore industry, the exploitation of offshore oil and gas resources moves to the deep water. In the real sea, strong nonlinear wave conditions may result in great harm to marine engineering structure. Extreme wave, which were known due to their exceptionally large height, steep shape, asymmetric wave form and unpredictability, can pose a serious threat to ships and offshore structures. Extreme waves generally are grouped, which are observed to be generated by accompanied with wind [6]. In the process of wave propagation, the wind energy is transferred to the wave group, which has a great influence on the wave evolution and its nonlinear characteristics. So it is very necessary to study the influence of wind on the evolution of extreme waves and its nonlinear characteristics. Liu et al. [4] presented an exploratory observational study of rogue waves based on wave measurement made in South Indian Ocean, and the effects of wind on the generation and propagation of extreme waves were studied. Touboul [14] numerically simulated the evolution of the extreme wave in the wind by the higher-order spectral method based on Jeffreys' sheltering mechanism and modulation instability. In addition, some numerical simulation methods have been established. De Angelis[1], Sullivan[9,10,11] and Nakayama[7] used the Navier-Stokes model to simulate the water flow on the surface. Kharif et al.[3] and Touboul et al. [12] introduced an additional air pressure on the free surface boundary conditions by considering Jeffreys' sheltering mechanism. Fulgosi et al. [2] established a Navier-Stokes equation based on the two-phase flow method, in which the interaction between wind and waves was fully considered. Yan and Ma [15] presented an improved model for evaluating air pressure acting on 2D extreme waves by analysing the pressure distribution over extreme waves using the QALE-FEM and StarCD approach.

As an extension of the previous studies, further investigations about the wind effect on the nonlinear characteristics of focused wave group were performed. A fully nonlinear time-domain higher-order boundary element method was developed to study the interaction of uniform wind and focused wave group. Then the influences of wind speed, wave spectrum and incident wave amplitude on the extreme wave properties under the action of wind is considered.

Numerical Model

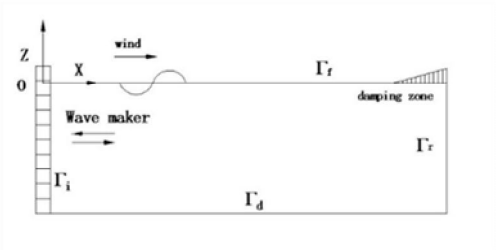

Figure.1. Definition sketch of the numerical flume

The interaction between extreme waves and wind in a 2D fluid domain is considered as shown in Figure.1. A Cartesian coordinate system *Oxz* is employed such that its origin locates on the still water level at the left end of the domain, and the z-axis is positive upward. It is assumed that the fluid is incompressible, inviscid and the flow motion irrotational so that a velocity potential exists in the fluid domain and velocity can be expressed as the following

$$\mathbf{v} = \nabla\phi \,, \mathbf{v} = (u, w) \tag{1}$$

The governing equation satisfies Laplace equation

$$\Delta\phi = 0 \,, \quad z < \eta(x,t) \tag{2}$$

The nonlinear kinematic and dynamic free surface boundary conditions is given as the following forms on the transient free surface

$$\frac{\partial \eta}{\partial t} = \frac{\partial \phi}{\partial z} - \frac{\partial \eta}{\partial x}\frac{\partial \phi}{\partial x} \tag{3}$$

$$\frac{\partial \phi}{\partial t} = -gz - \frac{p}{\rho} - \frac{1}{2}\left|\nabla\phi\right|^2 \tag{4}$$

In order to consider the wind influence, the pressure on the free surface in Eq.(4) is related to the local wave slope according to the following equation expressed by Kharif et al.[3] and Touboul et al.[12]

$$p = \rho_a s\left(U-c\right)^2 \frac{\partial \eta}{\partial x} \tag{5}$$

where the constant s is the sheltering coefficient; U the uniform wind speed; c the local wave phase velocity and ρ_a is atmospheric density. $s=0.5$ was determined from the previous researches [3, 12]. Here, a critical value of the local slope η_{x_c} is introduced, above which an energy transfer from the wind to the waves occurs. The critical value of the slope is chosen as 0.35 [3]. Then the pressure condition can be rewritten as follows:

$$\begin{cases} p(x) = 0 & if\ \eta_{x_{\max}} < \eta_{x_c} \\ p(x) = \rho_a s\left(U-c\right)^2 \dfrac{\partial \eta}{\partial x}(x) & if\ \eta_{x_{\max}} \geq \eta_{x_c} \end{cases} \tag{6}$$

The mixed Euler-Lagrangian scheme is used for tracing the fluid particle on the transient free surface in the present study. Thus, the material derivative is introduced and the kinematic free surface boundary condition is expressed as follows

$$\frac{Dx}{Dt} = \frac{\partial \phi}{\partial x}, \frac{Dz}{Dt} = \frac{\partial \phi}{\partial z} \tag{7}$$

On the flume bottom Γ_d, the rigid and impermeable boundary condition is satisfied as the following

$$\frac{\partial \phi}{\partial \mathbf{n}} = 0 \qquad on \quad \Gamma_d \tag{8}$$

Towards the end of the computational domain, an artificial damping beach is applied on the free surface so that the wave energy is gradually dissipated in the direction of the wave propagation. The profile and magnitude of the artificial damping have to be designed to minimize the possible wave reflection at the entrance of the damping zone. Then the free surface boundary conditions can be written as follows

$$\begin{cases} \dfrac{DX(x,z)}{Dt} = \nabla\phi - \mu(x)(X - X_0) \\ \dfrac{D\phi}{Dt} = -gz + \dfrac{1}{2}|\nabla\phi|^2 - \dfrac{p}{\rho} - \mu(x)\phi \end{cases} \tag{9}$$

where X_0 is the starting position of the damping layer. The damping function $\mu(x)$ is adopted as:

$$\mu(x) = \begin{cases} \omega_{\min}\left(\dfrac{x-x_0}{L_b}\right)^2, & x_0 \leq x \leq x_0 + L_b \\ 0, & x < x_0 \end{cases} \tag{10}$$

where $\omega_{\min}$ denotes the minimum angular frequency of the wave components and L_b is the length of the damping layer, and defined as $1.5\lambda_{\max}$ in the present study.

By applying Green's second identity to the above boundary value problem in the previous part, the boundary integral equation can be converted in the usual manner into the following

$$\alpha(p)\phi(p) = \int_\Gamma \left(\phi(q)\frac{\partial G(q,p)}{\partial n} - G(q,p)\frac{\partial \phi(q)}{\partial n}\right)d\Gamma \tag{11}$$

where $p=(x_0, z_0)$ and $q=(x, z)$ are source and field points, respectively. Γ denotes the boundary of the whole computational domain, and $\alpha(p)$ is the solid angle coefficient.

The boundary surface is discretized by the three-node line elements based on the quadratic shape functions. Within the boundary elements, physical variables are also interpolated by the same shape functions, i.e., the elements are isoparametric. Numerical integration over each boundary element is performed by using Gauss-Legendre quadrature with four integration points. Then the discretized integral equation is transformed into a system of linear algebraic equations. Since the discretized integral equation is always variant in time, all the boundary surface grids are updated at each time step using 4th-order Runga-Kutta approach. Once the Eq. (11) is solved, we can obtain the time series of surface elevation at any position [8].

Comparison with the Experiment

As a validation of the present model, numerical results are compared with the experiment performed by Kharif et al. [3]. The case considered here is about a 2D extreme wave under the action of wind. The length and depth of the flume are 40m and 1m, respectively. The extreme wave is generated by a wavemaker undergoing a sine motion based on the focused wave theory. The wave frequency varies linearly from the maximum frequency ($f_{\max}=1.85Hz$) to the minimum one ($f_{\min}=0.8Hz$) in a duration of T_0=23.5s. The piston-type wavemaker is used in the numerical simulation. The motion of the wavemaker is governed by the following equation

$$S(\tau) = \begin{cases} \dfrac{a}{F}\cos\left[\int_0^\tau \omega(\tau)d\tau\right] & \tau \leq T_0 \\ 0 & \text{else} \end{cases} \tag{12}$$

where a is the expected wave amplitude and given as 0.007, and F is transfer function of the wavemaker [5] which is given as follows

$$F = \frac{2\left[\cosh(2kh)-1\right]}{\sinh(2kh)+2kh} \tag{13}$$

where h is the static water depth. Wave number k and angular frequency ω satisfy the linear dispersion relation.

Figure 2 displays the time series of the experimental and numerical surface elevations at fetch $x=1m$, in which the numerical spatial and temporal steps are defined as $\Delta x=\lambda_{min}/20$ and $\Delta t=T/50$, respectively. The data at fetch $x=1m$ are in excellent agreement between two results while the discrepancies are observed at the starting position due to the difference of ramping functions.

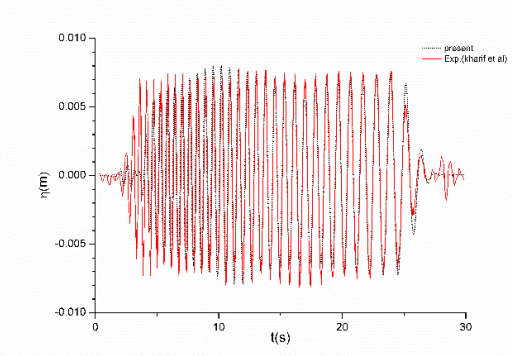

Figure 2. Time series of surface elevation at fetch x=1m (experimental data - solid line and numerical results - dashed line

Figure 3 shows the time series of the surface elevations at three fetches (i.e., x=11m, 18m and 21m), measured experimentally and computed numerically. The equilibrium positions of the surface elevation corresponding to fetches x=18m and x=21m are located at 0.05 and 0.1 respectively. From the figure, it can be seen that both the amplitudes and phases of the numerical and

experimental wave trains are quite similar, demonstrating the accuracy and efficiency of the proposed numerical model to reproduce correctly the nonlinear evolution of wave groups during the focusing-defocusing cycle.

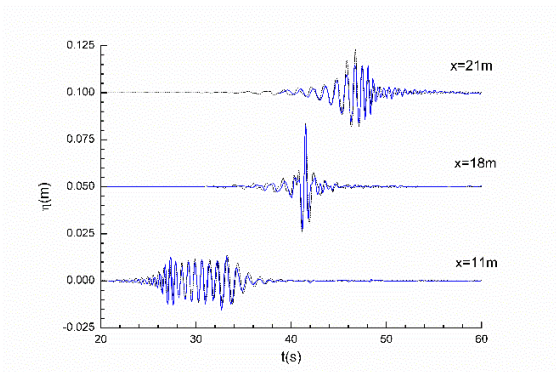

Figure 3.Time series of surface elevations at three fetches x=21m, x=18m, x=11m (experiments -solid line and numerical simulation-dashed line)

Numerical Results and Discussions

The nonlinear interaction between winds and 2D focused wave group is further studied in this section. In the numerical simulation, the focused wave group is generated using a sum of a number of sine wave components. The displacement of the wavemaker is given by

$$S(\tau)=\sum_{i=1}^{N}\frac{a_i}{T_r}\sin(k_i x_p+\omega_i(t-t_p)) \tag{14}$$

where T_r is the transfer function, which is determined as follows

$$T_r=\frac{4\sinh^2(k_i h)}{\left(2k_i h+\sinh(2k_i h)\right)} \tag{15}$$

where N=29 is the total number of components and k_i , ω_i are the wave number and frequency of the *i-th* component, respectively, which are related to each other by $\omega_i^2=gk_i\tanh(k_i h)$. a_i is the amplitude of *i-th* wave component, which is taken as the same for all components. The simple relationship between target amplitude (A_i) and the amplitudes of the components is $a_i=A_i/N$. Wave components are equally spaced within the appropriate wave period range. In the numerical simulation, two cases, i.e. 0.6s≤T≤1.4s and 0.8s≤T≤1.2s, are considered. The former case represents a wide spectrum bandwidth and the latter case represents a narrow spectrum bandwidth. The linear focal position and focal time are defined as x_p=6.5λ_{min} and t_p=16.5T_{min} respectively (λ_{min} and T_{min} denote the shortest wavelength and smallest wave period of wave components, respectively). The input wave target amplitudes A_i=0.05m and 0.06m are used here.

Figure 4 shows the distribution of focused wave amplitude under the action of different wind speeds with narrow and wide spectrum bandwidth, respectively. For the convenient comparison, the focused wave amplitude is nondimensionalized by A_i. It is observed that dimensionless extreme wave amplitude has a significant increase as the wind speed increases. This is due to more energy transferred from wind into the waves group that leads to the increase of the peak value. In addition, the value A/A_i increases faster for the larger wave amplitude. Compared with A_i=0.05m, the dimensionless maximum amplitude has a more significant increase due to higher and steeper wave crest in the case of A_i=0.06m. Frequency bandwidth is also one of the important factors influencing the characteristic of the extreme wave. The dimensionless focused wave amplitude is larger with the same wind speed in the case of narrow spectrum bandwidth, which shows stronger nonlinearity.

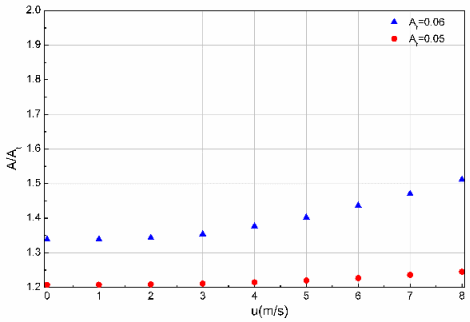

(a) 0.6s≤T≤1.4s

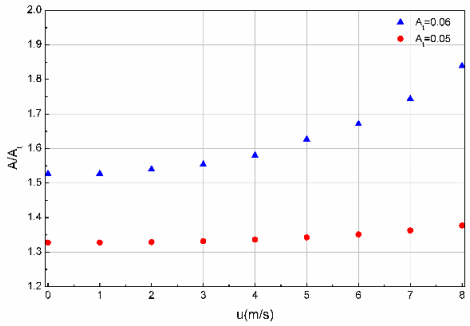

(b) 0.8s≤T≤1.2s

Figure 4. The dimensionless focusing wave amplitude as a function of wind speed

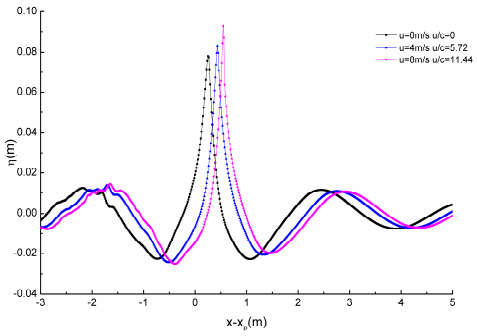

(a) 0.6s≤T≤1.4s, A_i=0.06m

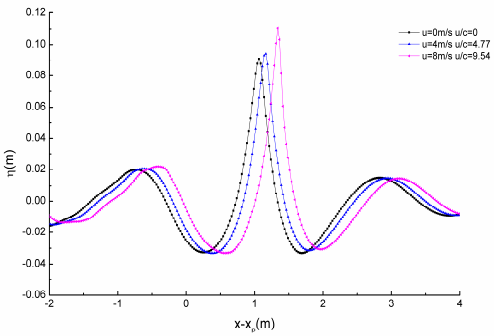

(b) 0.8s≤T≤1.2s, A_i=0.06m

Figure 5. Time series of surface elevations at the focal time with different wind speeds of 0, 4 and 8m/s

By taking A_i=0.06m as an example, Figure 5 shows the surface elevation at the focusing time on wind speeds of 0, 4 and 8m/s, respectively. For the convenience, a simple shift of the horizontal coordinate is carried out by subtracting the linear focal position x_p. It is obviously observed that the focused wave amplitude increases with the increase of wind speed. This figure also shows the the wind can further increase the shifts of focal position downstream the flume.

Figure 6 gives the deviation of the real focal position from the linear one as a function of the wind velocity. For the case of small amplitude A_i=0.05m, the focal position basically has no changes for different wind speed. However, for the case of large amplidtude A_i=0.06m, the wind weakly shifts the focusing point downstream, which can be also observed in figure 5. The same phenomenon was also found in the experiments of Kharif [3] and Touboul et al. [12], which is due to the action of the current induced by the wind. The input target wave amplitude plays an important role in the results. The Jeffreys' sheltering mechanism describes air flow separation over waves. This mechanism is not applicable for the gentle waves. However, for the steep wave, it is well known that air flow separation occurs, resulting in a significant increase of wind to wave energy [13].

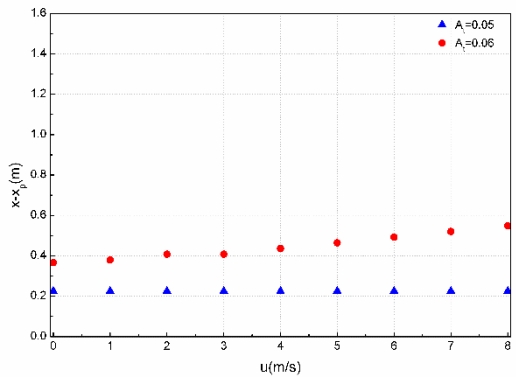

(a) 0.6s≤T≤1.4s

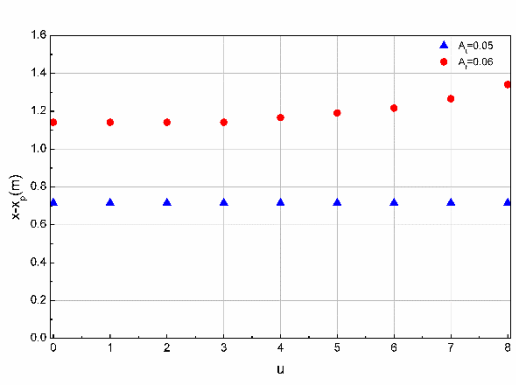

(b) 0.8s≤T≤1.2s

Figure 6. Distribution of the real focal position deviation from the input ones with wind velocity

Conclusions

In this paper, the influence of wind on the characteristics of a 2D dispersive focused wave group is investigated using a fully nonlinear numerical flume model, in which the modified Jeffreys' sheltering mechanism model is used to take into account of the wind pressure effect. Good agreements of the predicted results with the other published data are given to validate the proposed numerical model. Numerical investigations demonstrate that the action of wind can increase the extreme wave amplitude of focused wave group. The wind weakly shifts the focusing position downstream, which is due to the action of the current induced by the wind. Both narrow spectrum and larger input target amplitude have more significant influences on the extreme wave under the condition of wind.

Acknowledgements

The authors would like to gratefully acknowledge the financial support from the National Science Foundation of China (Grant Nos. 51679036, 51490672) and the Program for New Century Excellent Talents in University (Grant No.NCET-13-0076).

References

[1]. Angelis, V. D., Lombardi, P., & Banerjee, S. (1997). Direct numerical simulation of turbulent flow over a wavy wall. *Physics of Fluids, 9*(9), 2429-2442.

[2]. Fulgosi, M., Lakehal, D., Banerjee, S., & De Angelis, V. (2003). Direct numerical simulation of turbulence in a sheared airwater flow with a deformable interface. *Journal of Fluid Mechanics, 482*(1), 319-345.

[3]. Kharif, C., Giovanangeli, J. P., Touboul, J., Grare, L., & Pelinovsky, E. (2008). Influence of wind on extreme wave events: experimental and numerical approaches. *Journal of Fluid Mechanics, 594*(1), 209-247.

[4]. Liu, P. C., Machuchon, K. R., & Wu, C. H. (2004). Exploring rogue waves from observations in south indian ocean. *Actes de colloques - IFREMER, 39*.

[5]. Ma, Q. W. (2007). Numerical generation of freak waves using mlpg r and qale-fem methods. *Computer Modeling in Engineering & Sciences,18*(3), 223-234.

[6]. Mori, N., Liu, P. C., & Yasuda, T. (2002). Analysis of freak wave measurements in the sea of japan. *Ocean Engineering, 29*(11), 1399-1414.

[7]. Nakayama, A., Sakio, D. K., Nakayama, A., & Sakio, D. K. (2002). Simulation of flows over wavy rough boundaries. *Center for Turbulent Research, 313*.

[8]. Ning, D. Z., & Teng, B. (2007). Numerical simulation of fully nonlinear irregular wave tank in three dimension. *International Journal for Numerical Methods in Fluids,53*(12), 1847-1862.

[9]. Sullivan P P, Edson J B,Mcwilliams J C,et al. Large-eddy simulations and observations of wave-driven boundary layers[C].In Proc. 16th Symp. on Boundary Layers and Turbulence,Portland, 2004.

[10]. Sullivan, P. P., McWilliams, J. C., & Moeng, C. H. (2000). Simulation of turbulent flow over idealized water waves. *Journal of Fluid Mechanics*, 404, 47-85.

[11]. Sullivan, P. P., & Mcwilliams, J. C. (2002). Turbulent flow over water waves in the presence of stratification. *Physics of Fluids,14*(3), 1182-1195.

[12]. Touboul, J., & Giovanangeli, J. P. (2006). Freak waves under the action of wind: experiments and simulations. *European Journal of Mechanics B Fluids,25*(5), 662–676.

[13]. Touboul, J., Kharif, C., Pelinovsky, E., & Giovanangeli, J. P. (2008). On the interaction of wind and steep gravity wave groups using miles' and Jeffreys' mechanisms. *Nonlinear Processes in Geophysics,15*(6), 1023-1031.

[14]. Touboul, J. (2007). On the influence of wind on extreme wave events. *Natural Hazards & Earth System Sciences,7*(1), 123-128.

[15]. Yan, S., & Ma, Q. W. (2010). Numerical simulation of interaction between wind and 2d freak waves. *European Journal of Mechanics - B/Fluids,29*(1), 18–31.